Calibration Enhanced Decision Maker: Towards Trustworthy Sequential Decision-Making with Large Sequence Models

Anonymous authors
Paper under double-blind review

Abstract

Offline deep reinforcement learning (offline DRL) has attracted considerable attention across various domains due to its ability to learn effective policies without direct environmental interaction. Although highly effective, the trustworthiness of agent remains a paramount concern within the community. Offline DRL can be categorized into three principal paradigms: model-based algorithms, model-free algorithms, and trajectory optimization. While extant research predominantly concentrates on calibration enhancement of model-based and model-free algorithms, calibration of trajectory optimization remains a comparatively underexplored avenue of investigation. In this paper, we pioneer the concept of Expected Agent Calibration Error (EACE), a novel metric designed to assess agent calibration. Furthermore, we rigorously prove its theoretical relationship to the state-action marginal distribution distance. Subsequently, we introduce the Calibration Enhanced Decision Maker (CEDM), which employs a binning executor to process feature distribution histograms as input for the large sequence model, thereby minimizing the state-action marginal distribution distance and enhancing the agent's calibration. A series of in-depth case studies are undertaken to examine CEDM, with its application examined across Decision Transformer, Decision ConvFormer, and Decision Mamba. Empirical results substantiate the robustness of EACE and demonstrate the effectiveness of CEDM in enhancing agent calibration, thereby offering valuable insights for future research on trustworthy sequential decision-making.

1 Introduction

"A good decision is based on knowledge and not on numbers."

—— *Plato*

Deep reinforcement learning (DRL), employing the trial-and-error mechanisms to learn and optimize specific reward signals, has emerged as a powerful learning strategy executing autonomous data collection across various domains, such as robotic motion control (Singh et al., 2022; Tang et al., 2024), autonomous driving (Kiran et al., 2021; Zhao et al., 2024), large language model fine-tuning (Ouyang et al., 2022; Guo et al., 2025), and so on. Furthermore, it is the aspiration of many roboticists to program a robot with a task in the evening and return the following morning to discover it capable of effectively solving the task. Then, offline deep reinforcement learning (offline DRL) has garnered considerable interest in the community (Gürtler et al., 2023), primarily on account of its capacity to acquire effective strategies without the need for interaction with the environment. Such capability is particularly advantageous in scenarios where the cost or risk associated with real-time environmental engagement is substantial. According to survey compiled by Prudencio et al., it can be classified into three primary aspects: *(1) model-based algorithms* (Luo et al., 2024), *(2) model-free algorithms* (Swazinna et al., 2022), *(3) trajectory optimizations* (Janner et al., 2021; Hu et al., 2024).

Meanwhile, trustworthiness of the agent has also standed as a paramount concern within the community (Yu et al., 2025). It is widely acknowledged that miscalibrated trust can lead to misuse of agents (Wei et al., 2025). Therefore, to foster trustworthy and reliable agents, it is imperative to emphasize their calibration. In the aforementioned taxonomy of offline DRL, the first two categories already have corresponding works that

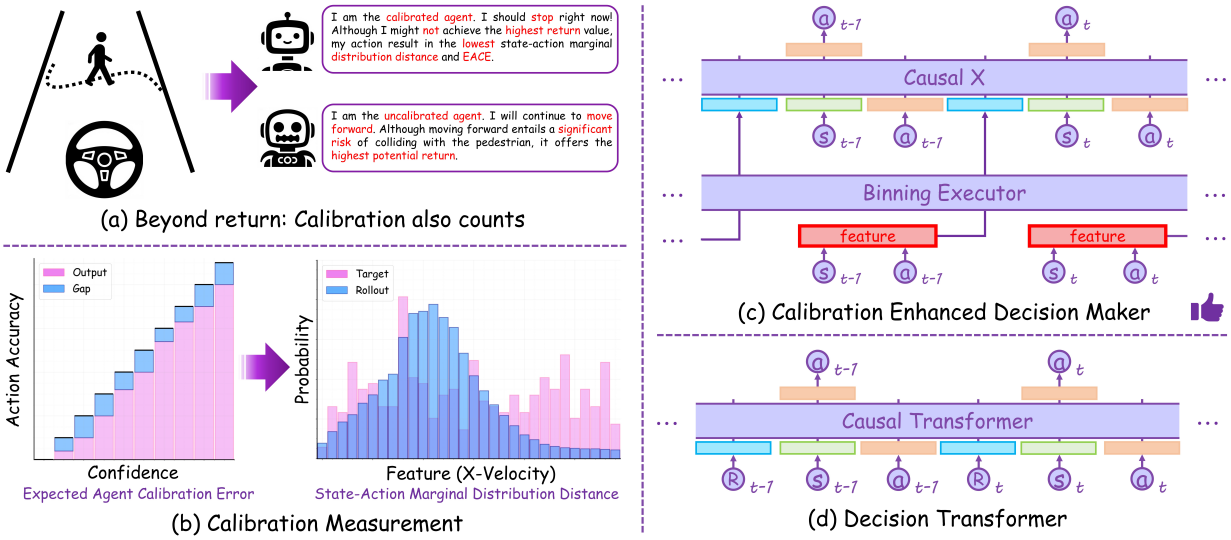

Figure 1: **(a) Motivation:** In real-world applications, especially in high-risk scenarios, trustworthiness of an agent's actions is also of great importance. **(b) Measurement:** We define the Expected Agent Calibration Error (EACE); furthermore, for practical applications, we theoretically establish the relationship between the EACE and the state-action marginal distribution distance. **(c) Methodology:** We introduce the Calibration Enhanced Decision Maker (CEDM) paradigm, which employs a binning executor to process the distribution histograms as inputs to the large sequence model. **(d) Prototype:** Decision Transformer has been a groundbreaking approach in offline DRL that treats decision-making as a sequence modeling problem.

consider calibration. Calibrated model-based DRL (Malik et al., 2019) demonstrates a method for endowing agents with a calibrated world model that accurately represents true uncertainty and enhances planning in high-stakes scenarios. Calibrated Q-learning (Cal-QL) (Nakamoto et al., 2024) learns conservative value functions (Kumar et al., 2020) that are calibrated with respect to behavior policy. However, current research on trajectory optimization has never incorporated calibration considerations, which poses a risk of misuse in future real-world applications. In this study, we primarily concentrate on offline DRL algorithms with large sequence models (such as Transformer (Vaswani, 2017), MetaFormer (Yu et al., 2022) and Mamba (Gu & Dao, 2024)). Therefore, we rise the following question:

Major Question

Can we enhance calibration of offline DRL algorithms that utilize large sequence models to further bolster their trustworthiness in future real-world applications?

To address this question, it is essential to first define a more accurate metric for agent calibration. Drawing inspiration from the definition of Expected Calibration Error (ECE) (Guo et al., 2017) in prior model calibration literature, we introduce the *Expected Agent Calibration Error (EACE)* as a rigorous metric to quantitatively characterize the calibration properties of agents. Nonetheless, implementing measurement in practical assessments is challenging due to safety concerns. Therefore, we further theoretically prove the relationship between the EACE and the state-action marginal distribution distance: *differences in the EACE are bounded by the total variation distance between the state-action marginal distributions of two agents; and under mild assumptions, this can be extended to the Wasserstein-1 distance.* In other words, a smaller Wasserstein-1 distance between the state-action marginal distributions of two agents indicates a smaller difference in their EACE values, implying superior agent calibration.

Based on these foreshadowings, we introduce the *Calibration Enhanced Decision Maker (CEDM)*. Unlike traditional approaches that rely solely on the "number" of return-to-go as input for the large sequence model, CEDM incorporates a binning executor to process feature distribution histograms, thereby providing richer "knowledge" for the agent. Intuitively, CEDM enables the agent under training to more accurately

model the state-action marginal distribution represented in the offline dataset. By minimizing the distance of the distributions, it consequently decreases the differences in the EACE, thereby enhancing agent calibration. Such paradigm is partially inspired by the previous studies on state-marginal matching (SMM) (Lee et al., 2019; Ghasemipour et al., 2020): they conduct a qualitative assessment of distribution matching outcomes within designated state dimensions (e.g. xy-positions); furthermore, it can be extended to the velocity (e.g. x-velocity) to obtain richer "knowledge". Categorical Decision Transformer (Furuta et al., 2022) has shown the potential of a similar paradigm within the Transformer architecture and has explained its effectiveness from the perspective of hindsight information matching (HIM). Moreover, we demonstrate the applicability of such paradigm to a wider range of large sequence models, which reduces the distance between state-action marginal distributions and thereby enhances the agent calibration.

Furthermore, we perform case studies by applying the CEDM paradigm to *Decision Transformer* (Chen et al., 2021), *Decision ConvFormer* (Kim et al., 2024), and *Decision Mamba* (Ota, 2024). Based on a comprehensive review of these practical implementations, several conclusions can be drawn. Firstly, the CEDM paradigm effectively decreases the Wasserstein-1 distance between the state-action marginal distributions of the target rollout and the agent's behavior. Secondly, performance of the agent (final return) can be improved by utilizing the CEDM paradigm. Finally, application of the CEDM paradigm to ultra-long context sequence models (e.g., Mamba) may encounter limitations inherent in the offline dataset itself, providing insights for future efforts to deploy more advanced sequence models in decision-making tasks.

In summary, our contributions are as follows:

- We introduce the agent calibration metric: Expected Agent Calibration Error (EACE). Furthermore, to facilitate practical implementation, we theoretically establish the relationship between the EACE and the state-action marginal distribution distance.

- We introduce the Calibration Enhanced Decision Maker (CEDM) paradigm, which utilizes a binning executor to process distribution histograms as inputs to the large sequence model. This paradigm effectively reduces the state-action marginal distribution distance, thereby enhancing the agent's calibration. To the best of our knowledge, this is the first study on the enhancement of agent calibration in the field of offline DRL with large sequence models.

- We perform case studies, applying the CEDM paradigm to Decision Transformer, Decision ConvFormer, and Decision Mamba. Experimental results demonstrate the effectiveness of CEDM and provide insights into its future applications in more advanced sequence models.

2 Related Work

2.1 Offline DRL with Large Sequence Models

Decision Transformer (Chen et al., 2021) represents a pioneering stride in reinforcement learning, reframing the decision-making as sequence modeling using the Transformer architecture to predict optimal actions by processing trajectories of state, action, and return-to-go (RTG). Such an innovative training paradigm has sparked a burgeoning trend in leveraging advanced large sequence models to address decision-making tasks. Decision ConvFormer (DC) (Kim et al., 2024) utilizes the architectural framework of MetaFormer (Yu et al., 2022), employing localized convolutional filtering as the token mixer, adeptly capturing the intrinsic local dependencies within the trajectories. Decision S4 (DS4) (David et al., 2023) employs an RNN-like S4 (Gu et al., 2022) architecture for inference, while Decision Mamba (DMamba) (Ota, 2024) directly substitutes the attention mechanism with Mamba (Gu & Dao, 2024). Furthermore, this paradigm has also been increasingly applied in various domains, including robotic motion control (Gajewski et al., 2024), autonomous driving (Li et al., 2025), and large language model fine-tuning (Hu et al., 2023). Despite the highly promising results of these endeavors, none of them have addressed the issue of agent calibration, thereby posing a significant risk to their reliability and trustworthiness in further real-world applications.

2.2 Model Calibration

Model calibration refers to the alignment between a model's predicted probabilities and the true likelihood of the events (Guo et al., 2017). For example, if the model assigns a 70% confidence level to a prediction, we would expect the predicted outcome to occur in approximately 70% of instances in practical application. Unlike accuracy, calibration emphasizes trustworthiness of confidence, tackling challenges such as overconfidence. This guarantees probabilistic reliability, which is of paramount importance in high-cost and high-stakes domains. The concept of calibration has found purchase in a multitude of domains, such as autonomous driving (Fu et al., 2012), computer vision (Guo et al., 2017), natural language processing (Zhao et al., 2021), and so on.

In the domain of offline DRL, researchers have also made significant strides in enhancing calibration. In the survey (Prudencio et al., 2023), offline DRL can be classified into three primary aspects: model-based algorithms, model-free algorithms, and trajectory optimizations. Calibrated model-based reinforcement learning, as detailed in (Malik et al., 2019), provides agents with a refined world model that accurately reflects inherent uncertainty, thereby improving planning in high-stakes scenarios. Calibrated Q-learning (Cal-QL) (Nakamoto et al., 2024) leverages a modified CQL framework to ensure learned policy Q-values remain above a lower bound and below upper bounds for suboptimal reference policies, thereby calibrating the learned Q-values to a reasonable scale. They have shown promising applications of calibration in both model-based and model-free algorithms; however, there is still a lack of effort to enhance calibration in trajectory optimizations. In this study, we aim to provide insights into bridging this gap.

3 Preliminaries

3.1 Offline DRL with Trajectory Optimization

In the scenario of offline DRL, our target is to identify an optimal policy $\pi^*(a|s)$, maximizing the expected cumulative reward $\mathbb{E}[\Sigma_{t=0}^{T} r_t]$. The state s_t and the action a_t are dictated by the behavior policy; while the next state s_{t+1} and the reward r_t are determined by the transition dynamics function. This enables the construction of an offline trajectory dataset $\tau = \{(s_t, a_t, s_{t+1}, r_t)_i\}$, where i presents the timestep in the episode. Trajectory optimization methods recast the goal as minimizing the action reconstruction loss due to the lack of interaction with the environment:

$$\mathcal{L}_\theta = \mathbb{E}_{(R,s,a)\sim\tau}[\frac{1}{T}\Sigma_{i=1}^{T}\mathcal{L}_{\text{MSE/CE}}(\hat{a}_t; a_t)], \tag{1}$$

where $\hat{a}_t = \pi(\cdot|s_{t-K+1:t}, R_{t-K+1:t}, a_{t-K:t-1})$ donates the reconstruction action; K is context length of the sequence model; $R_t = \Sigma_{t'=t}^{T} r_{t'}$ is the return-to-go (RTG). During the testing phase, a target RTG is manually predefined to encapsulate the intended performance benchmarks. Trajectories from last K timesteps are input into the model, which subsequently generates an action for the current timestep. Based on this, the environment provides the next state and reward, after which the RTG is updated accordingly. Then, these new elements are also input into the model.

3.2 Expected Calibration Error

Expected Calibration Error (ECE) (Naeini et al., 2015) has been a common metric for describing the calibration performance of models, which quantifies the discrepancy between the model's predicted confidence and its actual accuracy. A model is deemed as *"perfectly calibrated"* when there is a precise alignment between its confidence levels and its empirical performance:

$$\forall p \in [0,1], \mathbb{P}(\hat{Y} = Y|\hat{P} = p) = p,$$

where $\hat{Y}$ is the output of network prediction and $\hat{P}$ is its associated confidence (i.e. probability of correctness). Furthermore, the Expected Calibration Error (ECE) is defined as discrepancy between the empirical accuracy and the corresponding confidence level:

$$\text{ECE} = \mathbb{E}_{\hat{P}}\Big[\Big|\mathbb{P}\Big(\hat{Y} = Y|\hat{P} = p\Big) - p\Big|\Big]. \tag{2}$$

4 Methodology

In this section, we aim to address the challenge of enhancing agent calibration of offline DRL algorithms that utilize large sequence models, thereby improving their trustworthiness. Firstly, we introduce a metric called Expected Agent Calibration Error (EACE) to describe the agent calibration. Furthermore, we theoretically prove that the difference between EACE is bounded by the total variation distance and the Wasserstein-1 distance (under mild assumptions) between the learned policy and the hidden policy. Building upon them, we introduce Calibration Enhanced Decision Maker (CEDM), which further leverages the distribution histograms as input for the large sequence model, ultimately yielding the calibration enhanced agent.

4.1 Expected Agent Calibration Error

To address the aforementioned challenge, the first step is to formulate a precise description of agent calibration. Inspired by the concept of "perfect calibration" and incorporating the inherent mechanisms of offline DRL, we formally define the concept of "perfect policy calibration" in Definition 1:

Definition 1. *Defining $U = \mathbb{I}\left[dis\left(\pi_1, \pi_2\right) \leq \delta\right]$, where $\mathbb{I}(\cdot)$ is the the indicator function, $U = 1$ denotes that the distance between policy π_1 and policy π_2 is smaller than the threshold δ. Hence, for the agent (model), a perfect calibration (with full confidence) can be expressed as:*

$$\forall p \in [0,1], \mathbb{P}\left(\mathrm{U} = 1 | \hat{P} = p\right) = p. \tag{3}$$

Intuitively, "perfect policy calibration" refers to the scenario: two policies are sufficiently similar with the probability p; and exactly a proportion p of practical predictions are indeed sufficiently similar.

Building upon this and drawing inspiration from Expected Calibration Error (Guo et al., 2017), we define the Expected Agent Calibration Error (EACE) in Definition 2. Intuitively, EACE describes the average discrepancy between the agent's true probability p of "U=1" and the stated probability $\hat{P}$ when it asserts that "I am $\hat{P}$ confident that U=1":

Definition 2 (Expected Agent Calibration Error)**.** *Define the miscalibration of the agent by computing the expectation of calibration error over predicted confidence $\hat{P}$:*

$$\mathrm{EACE} = \mathbb{E}_{\hat{P}}\left[\left|\mathbb{P}(\mathrm{U} = 1 | \hat{P} = p) - p\right|\right]. \tag{4}$$

Nevertheless, we find that although EACE is theoretically complete and grounded, it is computationally impractical in real-world applications. Notably, in high-risk scenarios, particularly when the agent's true probability p is relatively low, such measurement become exceedingly costly.

Furthermore, as illustrated in Figure 1(d), in the context of offline DRL with large sequence models, the input tokens generally consist of states, actions, and their associated return-to-go values. Therefore, the subsequent action is essentially determined by the knowledge embedded in the preceding states and the preceding actions. This further inspires us to delve deeper into the relationship between the EACE and the state-action marginal distribution distance. Ultimately, we elaborate on this relationship in Theorem 1. Specifically, the differences in EACE are bounded by the total variation (TV) distance between the state-action marginal distributions of two agents, as formally expressed in Theorem 1.

Theorem 1. *Suppose $\pi_{\theta_1}(a|s)$ and $\pi_{\theta_2}(a|s)$ are separately two policies of two agents, $\rho^{\pi_{\theta_1}}(s,a)$ and $\rho^{\pi_{\theta_2}}(s,a)$ are the state-action marginal distributions of the two agents, then:*

$$\mathrm{EACE}(\pi_{\theta_1}) - \mathrm{EACE}(\pi_{\theta_2}) \leq \mathbb{E}\left[4 \cdot \mathrm{TV}\big(\rho^{\pi_{\theta_1}}(s,a), \rho^{\pi_{\theta_2}}(s,a)\big)\right], \tag{5}$$

where $\mathrm{TV}(\cdot)$ is the total variation distance.

Proof. Before presenting a detailed proof of Theorem 1, we first introduce two lemmas. The derivation of Lemma 1 primarily utilizes vector transformations and the absolute value inequality; and the derivation of Lemma 2 primarily relies on the Hölder's inequality. Their detailed proofs are provided in Appendix A.

Lemma 1. *Suppose a, b, c are three vectors, then we have that:*

$$\langle |a-b|, 2b\rangle - \langle |a-c|, 2c\rangle \leq \langle b + c + |a-b| + |a-c|, |b-c|\rangle . \tag{6}$$

Lemma 2. *a and b are two vectors, and each of their terms is nonnegative. Then, we can get:*

$$\langle a, b\rangle \leq \langle \|a\|_1, \|b\|_\infty \rangle , \tag{7}$$

where $\|a\|_1$ represents the L_1-norm of vector a and $\|b\|_\infty$ represents the L_∞-norm of vector b.

We now proceed to the proof of Theorem 1.

For any state-action marginal distribution, we set that $\hat{P} = p = \rho^{\pi_\theta}(s,a)$ without loss of generality. As $\rho^{\pi_\theta}(s,a) = \rho^{\pi_\theta}(s) \cdot \pi_\theta(a|s)$; and given policy π, the action is sampled with the policy $\pi_\theta(a|s)$. Thus, we have:

$$\begin{aligned}
\mathrm{EACE}(\pi_\theta) =& \mathbb{E}_{\hat{P}}\Big[\Big|\mathbb{P}(\mathrm{U}=1|\hat{P}=p, A=a) - p\Big|\Big] \\
=& \mathbb{E}_{\rho^{\pi_\theta}(s,a)}\Big[\Big|\mathbb{P}(\mathrm{U}=1|\hat{P}=\rho^{\pi_\theta}(s,a), A=a) - \rho^{\pi_\theta}(s,a)\Big|\Big] \\
=& \mathbb{E}\Big[\sum \rho^{\pi_\theta}(s,a)\Big|\mathbb{P}(\mathrm{U}=1|\hat{P}=\rho^{\pi_\theta}(s,a), A=a) - \rho^{\pi_\theta}(s,a)\Big|\Big].
\end{aligned} \tag{8}$$

We then abbreviate the conditional distribution $\mathbb{P}(\mathrm{U}=1|\hat{P}=\rho^{\pi_\theta}(s,a), A=a)$ as ρ^π. Then, we have:

$$\mathrm{EACE}(\pi_\theta) = \mathbb{E}\left[\langle |\rho^\pi - \rho^{\pi_\theta}(s,a)|, \rho^{\pi_\theta}(s,a)\rangle\right], \tag{9}$$

where $|\rho^\pi - \rho^{\pi_\theta}(s,a)|$ and $\rho^{\pi_\theta}(s,a)$ are vectors and $\langle |\rho^\pi - \rho^{\pi_\theta}(s,a)|, \rho^{\pi_\theta}(s,a)\rangle$ represents the inner product of $|\rho^\pi - \rho^{\pi_\theta}(s,a)|$ and $\rho^{\pi_\theta}(s,a)$. Further, let's compare the EACE of two agents $\theta_1, \theta_2 \in \Theta$:

$$\mathrm{EACE}(\pi_{\theta_1}) - \mathrm{EACE}(\pi_{\theta_2}) = \mathbb{E}\Big[\langle |\rho^\pi - \rho^{\pi_{\theta_1}}(s,a)|, \rho^{\pi_{\theta_1}}(s,a)\rangle - \langle |\rho^\pi - \rho^{\pi_{\theta_2}}(s,a)|, \rho^{\pi_{\theta_2}}(s,a)\rangle\Big]. \tag{10}$$

According to Lemma 1, we can get:

$$\begin{aligned}
&\mathrm{EACE}(\pi_{\theta_1}) - \mathrm{EACE}(\pi_{\theta_2}) \\
\leq& \mathbb{E}\Big[\Big\langle \frac{\rho^{\pi_{\theta_1}}(s,a) + \rho^{\pi_{\theta_2}}(s,a)}{2} + \frac{|\rho^\pi - \rho^{\pi_{\theta_1}}(s,a)| + |\rho^\pi - \rho^{\pi_{\theta_2}}(s,a)|}{2}, |\rho^{\pi_{\theta_1}}(s,a) - \rho^{\pi_{\theta_2}}(s,a)|\Big\rangle\Big].
\end{aligned} \tag{11}$$

According to the Lemma 2, we can have that:

$$\begin{aligned}
&\mathrm{EACE}(\pi_{\theta_1}) - \mathrm{EACE}(\pi_{\theta_2}) \\
\leq& \mathbb{E}\left[\left\langle \frac{\rho^{\pi_{\theta_1}}(s,a) + \rho^{\pi_{\theta_2}}(s,a) + |\rho^\pi(s,a) - \rho^{\pi_{\theta_1}}(s,a)| + |\rho^\pi(s,a) - \rho^{\pi_{\theta_2}}(s,a)|}{2}, |\rho^{\pi_{\theta_1}}(s,a) - \rho^{\pi_{\theta_2}}(s,a)|\right\rangle\right] \\
\leq& \mathbb{E}\left[\|\rho^{\pi_{\theta_1}}(s,a) - \rho^{\pi_{\theta_2}}(s,a)\|_1 \cdot \left\|\frac{\rho^{\pi_{\theta_1}}(s,a) + \rho^{\pi_{\theta_2}}(s,a) + |\rho^\pi(s,a) - \rho^{\pi_{\theta_1}}(s,a)| + |\rho^\pi(s,a) - \rho^{\pi_{\theta_2}}(s,a)|}{2}\right\|_\infty\right].
\end{aligned} \tag{12}$$

Setting that:

$$m(\pi_{\theta_1}, \pi_{\theta_2}, \pi) = \left\|\frac{\rho^{\pi_{\theta_1}}(s,a) + \rho^{\pi_{\theta_2}}(s,a) + |\rho^\pi(s,a) - \rho^{\pi_{\theta_1}}(s,a)| + |\rho^\pi(s,a) - \rho^{\pi_{\theta_2}}(s,a)|}{2}\right\|_\infty .$$

For the sake that each term of the distributions $\rho^{\pi_{\theta_1}}(s,a), \rho^{\pi_{\theta_2}}(s,a)$ and $\rho^\pi(s,a)$ are bounded in $[0,1]$; hence, it is evident that $m(\pi_{\theta_1}, \pi_{\theta_2}, \pi) \leq 2$. Therefore, we can get that:

$$\begin{aligned}
\mathrm{EACE}(\pi_{\theta_1}) - \mathrm{EACE}(\pi_{\theta_2}) &\leq \mathbb{E}\left[2 \cdot \|\rho^{\pi_{\theta_1}}(s,a), \rho^{\pi_{\theta_2}}(s,a)\|_1\right] \\
&= \mathbb{E}\left[4 \cdot \mathrm{TV}\left(\rho^{\pi_{\theta_1}}(s,a), \rho^{\pi_{\theta_2}}(s,a)\right)\right],
\end{aligned} \tag{13}$$

which completes the proof. □

Moreover, in practical applications, the Wasserstein-1 distance is often considered more applicable than the total variation distance, as it can better capture geometric properties of the distributions. Therefore, we extend the total variation distance in Theorem 1 to the Wasserstein-1 distance according to the inequality between them. Further defining the two policies as the anticipated ideal policy and the current policy, we can obtain the Proposition 1:

Proposition 1. *Suppose $\pi^*(a|s)$ is the anticipated ideal policy, $\pi_\theta(a|s)$ is the policy of the agent, $\rho^{\pi^*}(s,a)$ is the state-action marginal distribution of the anticipated ideal agent and $\rho^{\pi_\theta}(s,a)$ is the state-action marginal distribution of the current agent, then:*

$$\mathrm{EACE}(\pi_\theta) - \mathrm{EACE}(\pi^*) \leq \mathbb{E}\left[\frac{4}{d_{min}} \cdot \mathrm{W}_1\big(\rho^{\pi_\theta}(s,a), \rho^{\pi^*}(s,a)\big)\right], \tag{14}$$

where $\mathrm{W}_1\left(\rho^{\pi_\theta}(s,a), \rho^{\pi}(s,a)\right)$ represents the Wasserstein-1 distance between $\rho^{\pi_\theta}(s,a)$ and $\rho^{\pi}(s,a)$; let $\rho^{\pi_\theta}(s,a) \in \mu$ and $\rho^{\pi}(s,a) \in \nu$, setting $\Omega = supp(\mu) \cup supp(\nu)$, $d_{min} = \inf_{\rho^{\pi_\theta} \neq \rho^{\pi} \in \Omega} \|\rho^{\pi_\theta} - \rho^{\pi}\|$.

Proof. According to the work (Panaretos & Zemel, 2019), we introduce the following Lemma 3, which establishes relationship between the total variation (TV) distance and the Wasserstein-1 distance.

Lemma 3 ((Panaretos & Zemel, 2019))**.** *Setting X, Y are finitely discrete random variables, and they are bounded; $X \in \mu$ and $Y \in \nu$, $\Omega = supp(\mu) \cup supp(\nu)$; $d_{min} = \inf_{x \neq y \in \Omega} \|x - y\|$, then we have that:*

$$\mathrm{TV}\left(X, Y\right) \leq \frac{1}{d_{min}} \cdot \mathrm{W}_1(X, Y). \tag{15}$$

Herein, let's consider the proof of Proposition 1:

According to Theorem 1, we have that:

$$\mathrm{EACE}(\pi_\theta) - \mathrm{EACE}(\pi) \leq \mathbb{E}\left[4 \cdot \mathrm{TV}(\rho^{\pi_\theta}(s,a), \rho^{\pi}(s,a)\right].$$

According to Lemma 3, setting that $\rho^{\pi_\theta}(s,a) \in \mu$, $\rho^{\pi}(s,a) \in \nu$, $\Omega = supp(\mu) \cup supp(\nu)$, $d_{min} = \inf_{\rho^{\pi_\theta} \neq \rho^{\pi} \in \Omega} \|\rho^{\pi_\theta} - \rho^{\pi}\|$, we can derive that:

$$\begin{aligned} \mathrm{EACE}(\pi_\theta) - \mathrm{EACE}(\pi) &\leq \mathbb{E}\left[4 \cdot \mathrm{TV}(\rho^{\pi_\theta}(s,a), \rho^{\pi}(s,a)\right] \\ &\leq \mathbb{E}\left[\frac{4}{d_{min}} \cdot \mathrm{W}_1\left(\rho^{\pi_\theta}(s,a), \rho^{\pi}(s,a)\right)\right], \end{aligned} \tag{16}$$

which completes the proof. □

In summary, under mild assumptions, the EACE discrepancy between the anticipated ideal policy and the current policy is bounded by the Wasserstein-1 distance between their state-action marginal distributions. Hence, we can consider minimizing the upper bound, specifically the Wasserstein-1 distance, to reduce their EACE discrepancy.

4.2 Calibration Enhanced Decision Maker

Based on the comprehensive theoretical analysis presented above, we introduce Calibration Enhanced Decision Maker (CEDM) paradigm, which employs categorical state-action marginal distribution histograms as the input token to the large sequence model. As illustrated in Figure 1(c), a binning executor is utilized to transform the feature distribution into a categorical approximation of the original continuous distribution. Previous research has also explored the binning paradigm to enhance input information density: building upon prior work on the state-marginal matching (SMM) (Lee et al., 2019; Ghasemipour et al., 2020), the Categorical Decision Transformer (Furuta et al., 2022) demonstrates the potential of binning distributions, particularly reward distributions, within the Transformer architecture. Moreover, as demonstrated by our theoretical analysis, the CEDM paradigm can effectively enhance the agent's calibration and is applicable to all large sequence models instead of Transformer only.

Table 1: W1_Dis and return comparison of Calibration Enhanced Decision Transformer (CEDT) and Decision Transformer (DT). **Bolded text** indicates that the results of CEDT are superior to those of DT.

	CEDT					DT				
	W1_Dis ↓									
	Med	Med-Exp	Med-Rep	Average	Total	Med	Med-Exp	Med-Rep	Average	Total
HC	**0.19±0.01**	**0.68±0.29**	**0.31±0.03**	**0.39**		0.20±0.02	1.06±0.34	0.32±0.11	0.53	
Hp	**0.14±0.02**	**0.13±0.03**	**0.26±0.18**	**0.18**	**1.19**	0.14±0.02	0.13±0.03	0.70±0.18	0.32	1.39
Wk	**0.31±0.08**	**0.08±0.02**	1.46±0.80	0.62		0.43±0.11	0.08±0.04	1.12±0.62	0.54	
	Return ↑									
HC	42.77±0.26	**86.64±2.30**	**39.59±0.25**	**56.33**		42.88±0.29	84.05±2.52	39.09±0.39	55.34	
Hp	**59.85±0.52**	78.88±16.25	**62.11±17.96**	**70.96**	**200.27**	57.80±2.41	90.16±11.58	20.34±5.51	56.10	182.11
Wk	**73.77±4.28**	**107.70±0.70**	**37.48±17.83**	**72.98**		72.87±6.22	107.49±1.11	31.66±14.25	70.67	

Table 2: W1_Dis and return comparison of Calibration Enhanced Decision ConvFormer (CEDC) and Decision ConvFormer (DC). **Bolded text** indicates that the results of CEDC are superior to those of DC.

	CEDC					DC				
	W1_Dis ↓									
	Med	Med-Exp	Med-Rep	Average	Total	Med	Med-Exp	Med-Rep	Average	Total
HC	**0.20±0.05**	**0.46±0.25**	**0.09±0.04**	**0.25**		0.22±0.06	0.50±0.29	0.24±0.06	0.32	
Hp	**0.13±0.02**	**0.12±0.04**	**0.28±0.19**	**0.18**	**0.69**	0.15±0.03	0.15±0.07	0.93±0.33	0.41	1.16
Wk	**0.27±0.10**	**0.07±0.01**	**0.45±0.32**	**0.26**		0.46±0.13	0.23±0.31	0.60±0.22	0.43	
	Return ↑									
HC	**42.92±0.15**	**88.51±1.78**	**41.17±0.53**	**57.53**		42.81±0.22	88.16±2.53	39.69±0.21	56.89	
Hp	**62.67±1.62**	75.06±8.86	**75.14±13.39**	**70.96**	**204.75**	59.13±3.28	76.57±19.08	30.84±24.95	55.51	189.08
Wk	**76.09±2.56**	**108.05±0.76**	44.64±19.10	76.26		74.87±2.83	104.36±7.38	50.81±16.34	76.68	

Furthermore, as Plato stated, "a good decision is based on knowledge and not on numbers". The CEDM paradigm equips the agent with richer "knowledge", rather than relying solely on the "number" of return-to-go. In practical applications, agents can be endowed with different dimensions of "knowledge" according to the specific requirements of each task. For example, in autonomous driving, the planar velocity (x-velocity) should be prioritized for consideration; in obstacle-crossing robots, the vertical velocity (z-velocity) is also crucial; in robotic arms, the joint angular velocity is of primary importance; and in more elaborate applications, such as missile tracking or space robots, the acceleration should also be considered. The introduced CEDM paradigm enables further selection of the appropriate state-action marginal distribution for binning, thereby allowing customization to meet specific practical requirements.

5 Case Studies

This section presents case studies applying the CEDM paradigm to Decision Transformer (DT) (Chen et al., 2021), Decision ConvFormer (DC) (Kim et al., 2024), and Decision Mamba (DMamba) (Ota, 2024), with reports on final returns and the Wasserstein-1 distances between state-action marginal distributions to validate its effectiveness and enhancement on agent calibration. These three architectures represent three distinct

Table 3: W1_Dis and return comparison of Calibration Enhanced Decision Mamba (CEDMamba) and Decision Mamba (DMamba). **Bolded text** indicates that results of CEDMamba are superior to those of DMamba.

	CEDMamba					DMamba				
	W1_Dis ↓									
	Med	Med-Exp	Med-Rep	Average	Total	Med	Med-Exp	Med-Rep	Average	Total
HC	0.21±0.05	0.89±0.27	**0.11±0.04**	0.40		0.18±0.04	0.66±0.13	0.31±0.11	0.38	
Hp	0.15±0.03	**0.10±0.02**	**0.39±0.23**	**0.21**	**0.86**	0.14±0.03	0.15±0.02	0.65±0.18	0.31	1.33
Wk	**0.30±0.05**	**0.06±0.02**	**0.39±0.15**	**0.25**		0.50±0.18	0.88±0.25	0.55±0.27	0.64	
	Return ↑									
HC	42.87±0.23	85.59±2.05	**40.86±0.21**	**56.44**		42.97±0.12	86.73±1.29	39.26±0.54	56.32	
Hp	59.73±2.28	90.28±9.08	**78.19±2.12**	**76.07**	**212.94**	69.39±7.25	97.47±10.47	41.03±19.03	69.30	196.72
Wk	**76.69±2.40**	**108.05±1.00**	**56.56±5.12**	**80.43**		70.47±7.21	87.20±5.48	55.63±7.22	71.10	

levels of dependence on historical information within the decision-making process. We focus on investigating the following three questions:

1) Can the CEDM paradigm effectively reduce Wasserstein-1 distances, thereby enhance the agent's calibration?

2) Can the CEDM paradigm improve the agent's return?

3) Would the improvements of the CEDM paradigm be affected by different degrees of dependence on historical information during the decision-making process?

5.1 Experimental Setup

In our case studies, experiments are conducted with the OpenAI Gym environment (Brockman et al., 2016), MuJoCo tasks (Todorov et al., 2012), which serve as the most typical benchmark for reinforcement learning. Specifically, we utilize the task of HalfCheetah (**HC**), Hopper (**Hp**), Walker2d (**Wk**). In terms of datasets, we utilize medium (**Med**), medium-expert (**Med-Exp**), and medium-replay (**Med-Rep**) datasets that are from the D4RL benchmark (Fu et al., 2020). To ensure consistency, we utilize the distributions of x-velocity throughout our study. Furthermore, to facilitate a unified representation of returns across tasks, we perform normalization on the scores:

$$\text{Return} = 100 \times \frac{\text{Score} - \text{Random Score}}{\text{Expert Score} - \text{Random Score}}, \tag{17}$$

where the terms "Random Score" and "Expert Score" are adopted from the D4RL benchmark. When selecting the binning executor, we utilize the same binning method as that used in the Categorical Decision Transformer (Furuta et al., 2022). For each dataset in every task, we identify the best trajectory; and the results are reported as the "mean ± standard deviation" over five random seeds. Additionally, we calculate the **Average** performance for each task across the three corresponding datasets, as well as the **Total** results of the average values. The training hyperparameters and implementation details are consistent with those reported in the original paper.

5.2 Comparison Results

In Table 1, Table 2, and Table 3, we present the comparative results of Wasserstein-1 distance and return by applying the CEDM paradigm to Decision Transformer (DT), Decision ConvFormer (DC), and Decision

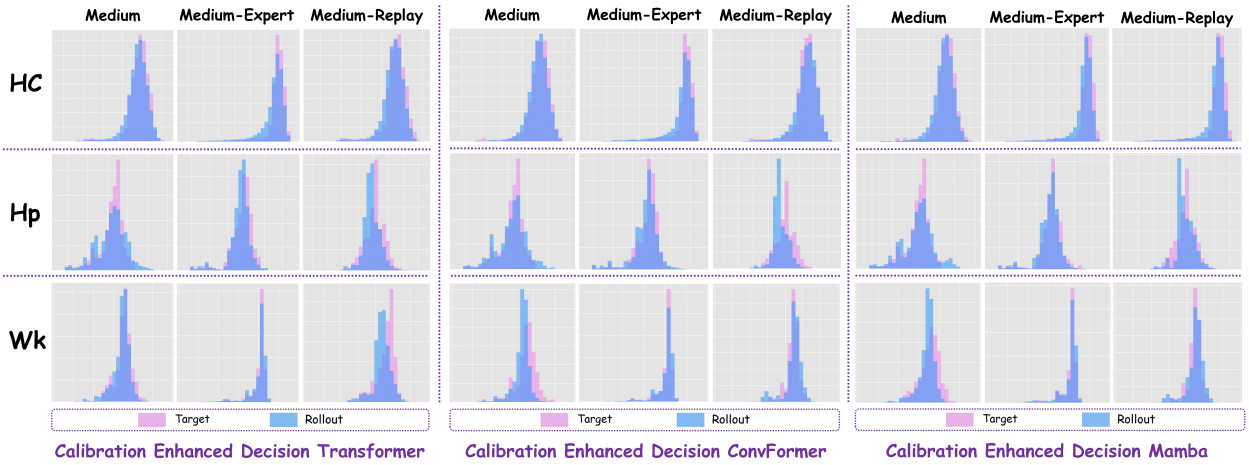

Figure 2: Visualizations of the distribution histograms for the highest-return trajectory of CEDT (*left*), CEDC (*middle*) and CEDMamba (*right*), presented separately for the three tasks across the three datasets.

Mamba (DMamba), respectively. Moreover, the three architectures represent distinct levels of dependence on historical information within the decision-making process: DC primarily utilizes local information, while DMamba emphasizes global information.

Firstly, we analyze the impact of the CEDM paradigm on the agents' Wasserstein-1 distances to address the first question. From an overall perspective, specifically in comparison to the "Total" values, it is indicated that the Calibration Enhanced Decision Makers effectively reduce the Wasserstein-1 distance across all architectural configurations relative to the baseline methods. To be specific, Table 1 demonstrates that CEDT achieves a reduction of 14.4% in the total Wasserstein-1 distance, decreasing it from 1.39 to 1.19; Table 2 indicates that CEDC attains a reduction of 40.5% in the total Wasserstein-1 distance, lowering it from 1.16 to 0.69; Table 3 reveals that CEDMamba accomplishes a reduction of 35.3% in the total Wasserstein-1 distance, reducing from 1.33 to 0.86. Consequently, the CEDM paradigm is empirically demonstrated to effectively reduce the Wasserstein-1 distance between state-action marginal distributions, thereby enhancing the agent calibration. Furthermore, to facilitate intuitive comprehension, we present representative visualizations of the distribution histograms for them, as depicted in Figure 2. Overall, the CEDM paradigm exhibits a good alignment with the distributions from the original dataset, thereby highlighting efficacy of CEDM paradigm.

Secondly, let's proceed to answer the second question. Although primary motivation of the CEDM paradigm is to enhance agent calibration, it is also crucial to evaluate its potential impact on the final return. By comparing the "Total" return values, it is evident that the Calibration Enhanced Decision Makers consistently outperform the baseline methods, yielding superior final returns across all architectural configurations. To be specific, Table 1 demonstrates that CEDT achieves an improvement of 10.0% in the total final return, elevating it from 182.11 to 200.27; Table 2 indicates that CEDC attains an improvement of 8.3% in the total final return, enhancing it from 189.08 to 204.75; Table 3 reveals that CEDMamba accomplishes an improvement of 8.2% in the total final return, raising it from 196.72 to 212.94. Notably, we observe that the improvements achieved by the CEDM paradigm are particularly pronounced on the Hopper-Medium-Replay dataset: specifically, CEDT exhibits an increase from 20.34 to 62.11; CEDC improves from 30.84 to 75.14; and CEDMamba demonstrates a rise from 41.03 to 78.19. According to the study (Ajay et al., 2023), the action trajectories in the Hopper-Medium-Replay dataset exhibit a propensity for diminished smoothness. Therefore, the CEDM paradigm is still capable of maintaining remarkable efficacy even when implemented on datasets of relatively lower quality.

Finally, we advance to answer the third question. Within the results, it is observed that the CEDM paradigm occasionally exhibits instances of failure, particularly in relation to CEDMamba. We argue that this phenomenon is attributable to the inherent ultra-long context capabilities of Mamba. In Figure 3, we present an

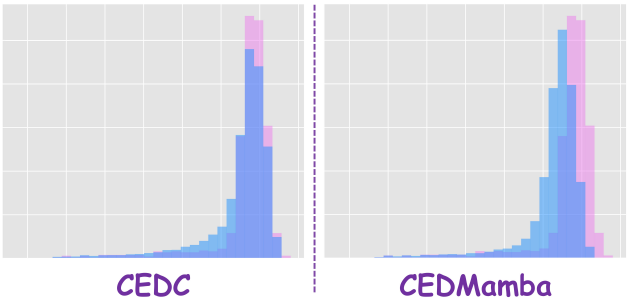

Figure 3: Example rollout (blue) visualizations of CEDC (*left*) and CEDMamba (*right*) on the HalfCheetah medium-expert dataset for the same target (violet).

example that demonstrates the differences in rollouts between CEDC and CEDMamba for the same target. For the CEDC, its convolutional architecture endows it with an enhanced capacity to capture local information, thereby exhibiting superior fitting performance within high-probability regions. However, CEDMamba predominantly emphasizes global information, thereby making its modeling of high-probability regions particularly vulnerable to biases stemming from the dataset. This further highlights two critical considerations for future real-world applications: firstly, the selection of an appropriate backbone should be tailored to the specific dataset and task; secondly, the quality of offline datasets plays a crucial role in shaping effectiveness of the CEDM paradigm.

6 Conclusion, Limitation, and Future Work

In this study, we focus on the crucial challenge of enhancing calibration in offline DRL algorithms that leverage large sequence models, with the aim of enhancing their trustworthiness in future real-world applications. We begin by introducing the Expected Agent Calibration Error (EACE), a metric that describes the agent calibration. Furthermore, to facilitate practical assessments, we rigorously establish its theoretical relationship with the state-action marginal distribution distance: the EACE discrepancy between the anticipated ideal policy and the current policy is bounded by the Wasserstein-1 distance between the agent's state-action marginal distributions under the two policies. Subsequently, we introduce the Calibration Enhanced Decision Maker (CEDM) paradigm, which leverages a binning executor to process distribution histograms as inputs to the large sequence model. This paradigm aims at reducing the discrepancy between state-action marginal distributions, thereby enhancing agent's calibration. Moreover, we perform case studies, applying the CEDM paradigm to Decision Transformer, Decision ConvFormer, and Decision Mamba. Experimental results highlight effectiveness of the CEDM paradigm and shed light on its future application in more advanced large sequence models.

Limitation. Although the CEDM paradigm has demonstrated significant advancements in trustworthiness and has exhibited promising performance across simulation environments, its effectiveness in real-world applications necessitates further investigation and exploration.

Future Work. Going forward, efforts in the future could primarily focus on the following three points. Firstly, the applications of the CEDM paradigm to real-world scenarios warrant further exploration, particularly in the domains of robotic motion control and autonomous driving. Secondly, it is also worthwhile to further investigate the applications of diverse physical quantities beyond velocity, such as joint angular velocity and acceleration, within the CEDM paradigm. Lastly, future research should continue to investigate approaches in the domain of trajectory optimization that could enhance agent calibration.

Broader Impact Statement

As stated in Section 4.2, the proposed CEDM paradigm allows flexible customization to meet specific practical requirements. Therefore, it holds great potential for real-world applications and is expected to be further extended to areas including robotics, autonomous driving, and aerospace engineering.

References

Anurag Ajay, Yilun Du, Abhi Gupta, Joshua B. Tenenbaum, Tommi S. Jaakkola, and Pulkit Agrawal. Is conditional generative modeling all you need for decision making? In *The Eleventh International Conference on Learning Representations*, 2023.

Greg Brockman, Vicki Cheung, Ludwig Pettersson, Jonas Schneider, John Schulman, Jie Tang, and Wojciech Zaremba. Openai gym. *arXiv preprint arXiv:1606.01540*, 2016.

Lili Chen, Kevin Lu, Aravind Rajeswaran, Kimin Lee, Aditya Grover, Misha Laskin, Pieter Abbeel, Aravind Srinivas, and Igor Mordatch. Decision transformer: Reinforcement learning via sequence modeling. *Advances in neural information processing systems*, 34:15084–15097, 2021.

Shmuel Bar David, Itamar Zimerman, Eliya Nachmani, and Lior Wolf. Decision s4: Efficient sequence-based RL via state spaces layers. In *The Eleventh International Conference on Learning Representations*, 2023.

Justin Fu, Aviral Kumar, Ofir Nachum, George Tucker, and Sergey Levine. D4rl: Datasets for deep data-driven reinforcement learning. *arXiv preprint arXiv:2004.07219*, 2020.

Xianping Fu, Xiao Guan, Eli Peli, Hongbo Liu, and Gang Luo. Automatic calibration method for driver's head orientation in natural driving environment. *IEEE Transactions on Intelligent Transportation Systems*, 14(1):303–312, 2012.

Hiroki Furuta, Yutaka Matsuo, and Shixiang Shane Gu. Generalized decision transformer for offline hindsight information matching. In *International Conference on Learning Representations*, 2022.

Paul Gajewski, Dominik Żurek, Marcin Pietroń, and Kamil Faber. Solving multi-goal robotic tasks with decision transformer. *arXiv preprint arXiv:2410.06347*, 2024.

Seyed Kamyar Seyed Ghasemipour, Richard Zemel, and Shixiang Gu. A divergence minimization perspective on imitation learning methods. In *Conference on robot learning*, pp. 1259–1277. PMLR, 2020.

Albert Gu and Tri Dao. Mamba: Linear-time sequence modeling with selective state spaces. In *First Conference on Language Modeling*, 2024.

Albert Gu, Karan Goel, and Christopher Re. Efficiently modeling long sequences with structured state spaces. In *International Conference on Learning Representations*, 2022.

Chuan Guo, Geoff Pleiss, Yu Sun, and Kilian Q Weinberger. On calibration of modern neural networks. In *International conference on machine learning*, pp. 1321–1330. PMLR, 2017.

Daya Guo, Dejian Yang, Haowei Zhang, Junxiao Song, Ruoyu Zhang, Runxin Xu, Qihao Zhu, Shirong Ma, Peiyi Wang, Xiao Bi, et al. Deepseek-r1: Incentivizing reasoning capability in llms via reinforcement learning. *arXiv preprint arXiv:2501.12948*, 2025.

Nico Gürtler, Sebastian Blaes, Pavel Kolev, Felix Widmaier, Manuel Wüthrich, Stefan Bauer, Bernhard Schölkopf, and Georg Martius. Benchmarking offline reinforcement learning on real-robot hardware. *arXiv preprint arXiv:2307.15690*, 2023.

Jian Hu, Li Tao, June Yang, and Chandler Zhou. Aligning language models with offline learning from human feedback. *arXiv preprint arXiv:2308.12050*, 2023.

Shengchao Hu, Li Shen, Ya Zhang, Yixin Chen, and Dacheng Tao. On transforming reinforcement learning with transformers: The development trajectory. *IEEE Transactions on Pattern Analysis and Machine Intelligence*, 2024.

Michael Janner, Qiyang Li, and Sergey Levine. Offline reinforcement learning as one big sequence modeling problem. *Advances in neural information processing systems*, 34:1273–1286, 2021.

Jeonghye Kim, Suyoung Lee, Woojun Kim, and Youngchul Sung. Decision convformer: Local filtering in metaformer is sufficient for decision making. In *The Twelfth International Conference on Learning Representations*, 2024.

B Ravi Kiran, Ibrahim Sobh, Victor Talpaert, Patrick Mannion, Ahmad A Al Sallab, Senthil Yogamani, and Patrick Pérez. Deep reinforcement learning for autonomous driving: A survey. *IEEE transactions on intelligent transportation systems*, 23(6):4909–4926, 2021.

Aviral Kumar, Aurick Zhou, George Tucker, and Sergey Levine. Conservative q-learning for offline reinforcement learning. *Advances in Neural Information Processing Systems*, 33:1179–1191, 2020.

Lisa Lee, Benjamin Eysenbach, Emilio Parisotto, Eric Xing, Sergey Levine, and Ruslan Salakhutdinov. Efficient exploration via state marginal matching. *arXiv preprint arXiv:1906.05274*, 2019.

Zenan Li, Fan Nie, Qiao Sun, Fang Da, and Hang Zhao. Uncertainty-aware decision transformer for stochastic driving environments. In *Conference on Robot Learning*, pp. 364–386. PMLR, 2025.

Fan-Ming Luo, Tian Xu, Hang Lai, Xiong-Hui Chen, Weinan Zhang, and Yang Yu. A survey on model-based reinforcement learning. *Science China Information Sciences*, 67(2):121101, 2024.

Ali Malik, Volodymyr Kuleshov, Jiaming Song, Danny Nemer, Harlan Seymour, and Stefano Ermon. Calibrated model-based deep reinforcement learning. In *International Conference on Machine Learning*, pp. 4314–4323. PMLR, 2019.

Mahdi Pakdaman Naeini, Gregory Cooper, and Milos Hauskrecht. Obtaining well calibrated probabilities using bayesian binning. In *Proceedings of the AAAI conference on artificial intelligence*, volume 29, 2015.

Mitsuhiko Nakamoto, Simon Zhai, Anikait Singh, Max Sobol Mark, Yi Ma, Chelsea Finn, Aviral Kumar, and Sergey Levine. Cal-ql: Calibrated offline rl pre-training for efficient online fine-tuning. *Advances in Neural Information Processing Systems*, 36, 2024.

Toshihiro Ota. Decision mamba: Reinforcement learning via sequence modeling with selective state spaces. *arXiv preprint arXiv:2403.19925*, 2024.

Long Ouyang, Jeffrey Wu, Xu Jiang, Diogo Almeida, Carroll Wainwright, Pamela Mishkin, Chong Zhang, Sandhini Agarwal, Katarina Slama, Alex Ray, et al. Training language models to follow instructions with human feedback. *Advances in neural information processing systems*, 35:27730–27744, 2022.

Victor M. Panaretos and Yoav Zemel. Statistical aspects of wasserstein distances. *Annual Review of Statistics and Its Application*, 6(1):405–431, March 2019. ISSN 2326-831X. doi: 10.1146/annurev-statistics-030718-104938.

Rafael Figueiredo Prudencio, Marcos ROA Maximo, and Esther Luna Colombini. A survey on offline reinforcement learning: Taxonomy, review, and open problems. *IEEE Transactions on Neural Networks and Learning Systems*, 2023.

Bharat Singh, Rajesh Kumar, and Vinay Pratap Singh. Reinforcement learning in robotic applications: a comprehensive survey. *Artificial Intelligence Review*, 55(2):945–990, 2022.

Phillip Swazinna, Steffen Udluft, Daniel Hein, and Thomas Runkler. Comparing model-free and model-based algorithms for offline reinforcement learning. *IFAC-PapersOnLine*, 55(15):19–26, 2022.

Chen Tang, Ben Abbatematteo, Jiaheng Hu, Rohan Chandra, Roberto Martín-Martín, and Peter Stone. Deep reinforcement learning for robotics: A survey of real-world successes. *Annual Review of Control, Robotics, and Autonomous Systems*, 8, 2024.

Emanuel Todorov, Tom Erez, and Yuval Tassa. Mujoco: A physics engine for model-based control. In *2012 IEEE/RSJ international conference on intelligent robots and systems*, pp. 5026–5033. IEEE, 2012.

A Vaswani. Attention is all you need. *Advances in Neural Information Processing Systems*, 2017.

Zeming Wei, Tianlin Li, Xiaojun Jia, Yihao Zhang, Yang Liu, and Meng Sun. Position: Agent-specific trustworthiness risk as a research priority. In *ICML 2025 Workshop on Reliable and Responsible Foundation Models*, 2025.

Miao Yu, Fanci Meng, Xinyun Zhou, Shilong Wang, Junyuan Mao, Linsey Pang, Tianlong Chen, Kun Wang, Xinfeng Li, Yongfeng Zhang, et al. A survey on trustworthy llm agents: Threats and countermeasures. *arXiv preprint arXiv:2503.09648*, 2025.

Weihao Yu, Mi Luo, Pan Zhou, Chenyang Si, Yichen Zhou, Xinchao Wang, Jiashi Feng, and Shuicheng Yan. Metaformer is actually what you need for vision. In *Proceedings of the IEEE/CVF conference on computer vision and pattern recognition*, pp. 10819–10829, 2022.

Rui Zhao, Yun Li, Yuze Fan, Fei Gao, Manabu Tsukada, and Zhenhai Gao. A survey on recent advancements in autonomous driving using deep reinforcement learning: Applications, challenges, and solutions. *IEEE Transactions on Intelligent Transportation Systems*, 2024.

Zihao Zhao, Eric Wallace, Shi Feng, Dan Klein, and Sameer Singh. Calibrate before use: Improving few-shot performance of language models. In *International conference on machine learning*, pp. 12697–12706. PMLR, 2021.

A Detailed Proof of Lemma 1 and Lemma 2

Lemma 1. *Suppose a, b, c are three vectors, then we have that:*

$$\langle |a-b|, 2b\rangle - \langle |a-c|, 2c\rangle \leq \langle b+c+|a-b|+|a-c|\,, |b-c|\rangle\,. \tag{18}$$

Proof. Consider the following inequation:

$$\langle |a-c|, b-c-|b-c|\rangle \leq \langle |a-b|, c-b+|c-b|\rangle \tag{19}$$

According to the nature of the absolute value, it is obvious that $b-c-|b-c| \leq 0$ and that $c-b+|c-b| \geq 0$, which shows the constancy of Equation (19) is obvious.
Transform Equation (19), we can get that:

$$\langle |a-c|, b\rangle + \langle |a-b|, b-|b-c|\rangle \leq \langle |a-c|, c+|b-c|\rangle + \langle c, |a-b|\rangle \tag{20}$$

Based on the absolute value inequality, we can get:

$$|a-b| - |b-c| \leq |a-c|; |a-c| + |b-c| \geq |a-b| \tag{21}$$

Hence, we have that:

$$\begin{aligned}\langle |a-b|-|b-c|, b\rangle + \langle |a-b|, b-|b-c|\rangle &\leq \langle |a-c|, b\rangle + \langle |a-b|, b-|b-c|\rangle \\ &\leq \langle |a-c|, c+|b-c|\rangle + \langle c, |a-b|\rangle \\ &\leq \langle |a-c|, c+|b-c|\rangle + \langle c, |a-c|+|b-c|\rangle\end{aligned} \tag{22}$$

Combine some items of the same kind:

$$\langle |a-b|-|b-c|, b\rangle + \langle |a-b|, b-|b-c|\rangle \leq \langle |a-c|+|b-c|, c\rangle + \langle |a-c|, c+|b-c|\rangle \tag{23}$$

Thus, we have that:

$$2\langle |a-b|, b\rangle - 2\langle |a-c|, c\rangle \leq \langle b, |b-c|\rangle + \langle c, |b-c|\rangle + \langle |a-b|, |b-c|\rangle + \langle |a-c|, |b-c|\rangle \tag{24}$$

Then, we have that:

$$\langle |a-b|, 2b\rangle - \langle |a-c|, 2c\rangle \leq \langle b+c+|a-b|+|a-c|\,, |b-c|\rangle\,, \tag{25}$$

which completes the proof. □

For the proof of Lemma 2, we rely on the following fact, which is also denoted as the Hölder's inequality.

Fact 1 (Hölder's inequality)**.** *Set $p > 1, 1/p + 1/q = 1$, if $a_1, a_2 ... a_n$ and $b_1, b_2 ... b_n$ is nonnegative, then we have:*

$$\sum_{i=1}^{n} a_i b_i \leq \left(\sum_{i=1} a_i^p\right)^{\frac{1}{p}} \left(\sum_{i=1} b_i^q\right)^{\frac{1}{q}} \tag{26}$$

Lemma 2. *a and b are two vectors, and each of their terms is nonnegative. Then, we can get:*

$$\langle a, b\rangle \leq \langle \|a\|_1, \|b\|_\infty\rangle\,, \tag{27}$$

where $\|a\|_1$ represents the L_1-norm of vector a and $\|b\|_\infty$ represents the L_∞-norm of vector b.

Proof. Setting p as ∞ and q as 1, then according to the Equation (26) (Hölder's inequality), we can have:

$$\sum_{i=1}^{n} a_i b_i \leq \|b\|_\infty \cdot \|a\|_1 \tag{28}$$

Thus, we have that:

$$\langle a, b\rangle \leq \langle \|a\|_1, \|b\|_\infty\rangle\,, \tag{29}$$

which completes the proof. □

B Additional Visualizations of the Distribution Histograms

In this section, we provide more visualizations of the distribution histograms of four additional trajectories. In each figure, each row represents results on the specific dataset: medium as **Med**; medium-expert as **Med-Exp**; medium-replay as **Med-Rep**.

Calibrated Enhanced Decision Transformer (CEDT): Figure 4 (HalfCheetah), Figure 5 (Hopper), Figure 6 (Walker2d).

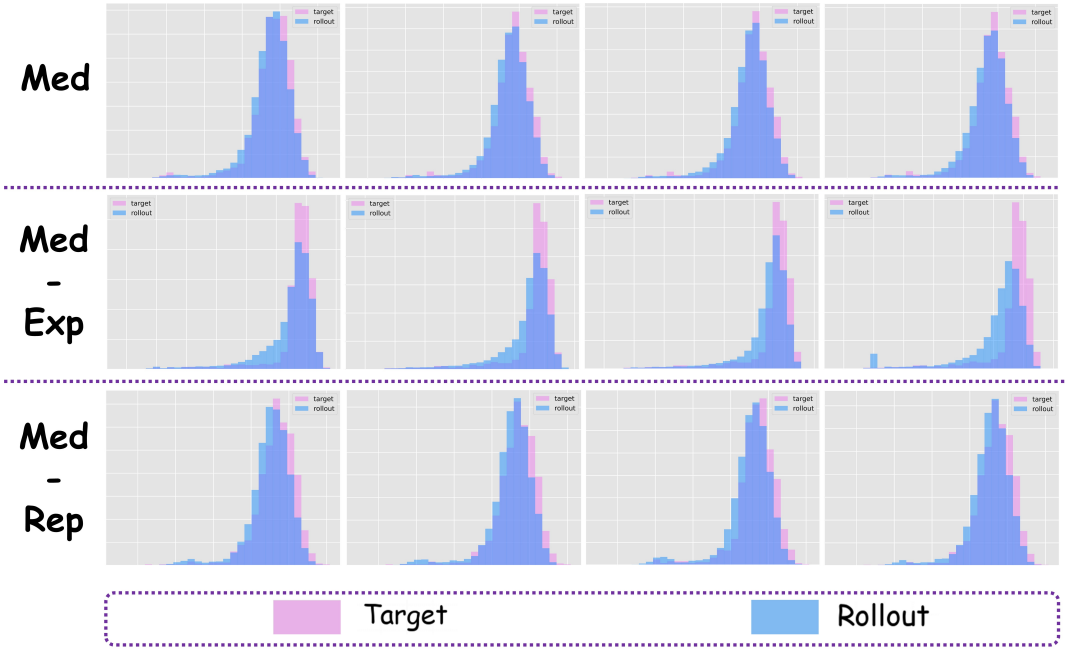

Figure 4: Within the **CEDT**, for the **HalfCheetah** task, additional visualizations of distribution histograms across three datasets.

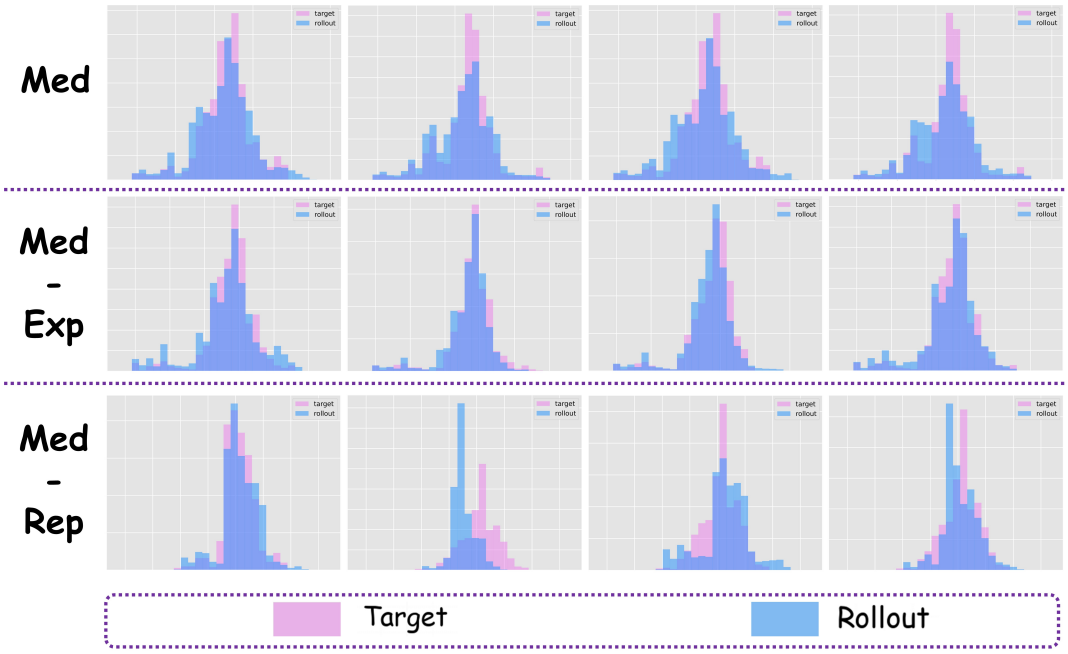

Figure 5: Within the **CEDT**, for the **Hopper** task, additional visualizations of distribution histograms across three datasets.

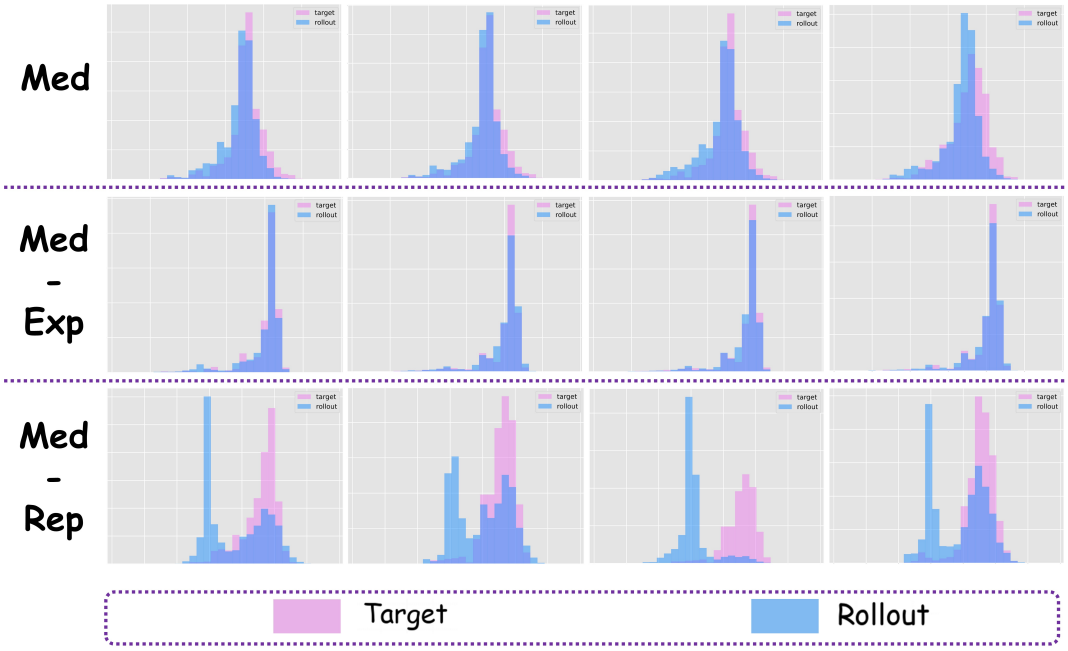

Figure 6: Within the **CEDT**, for the **Walker2d** task, additional visualizations of distribution histograms across three datasets.

Calibrated Enhanced Decision ConvFormer (CEDC): Figure 7 (HalfCheetah), Figure 8 (Hopper), Figure 9 (Walker2d).

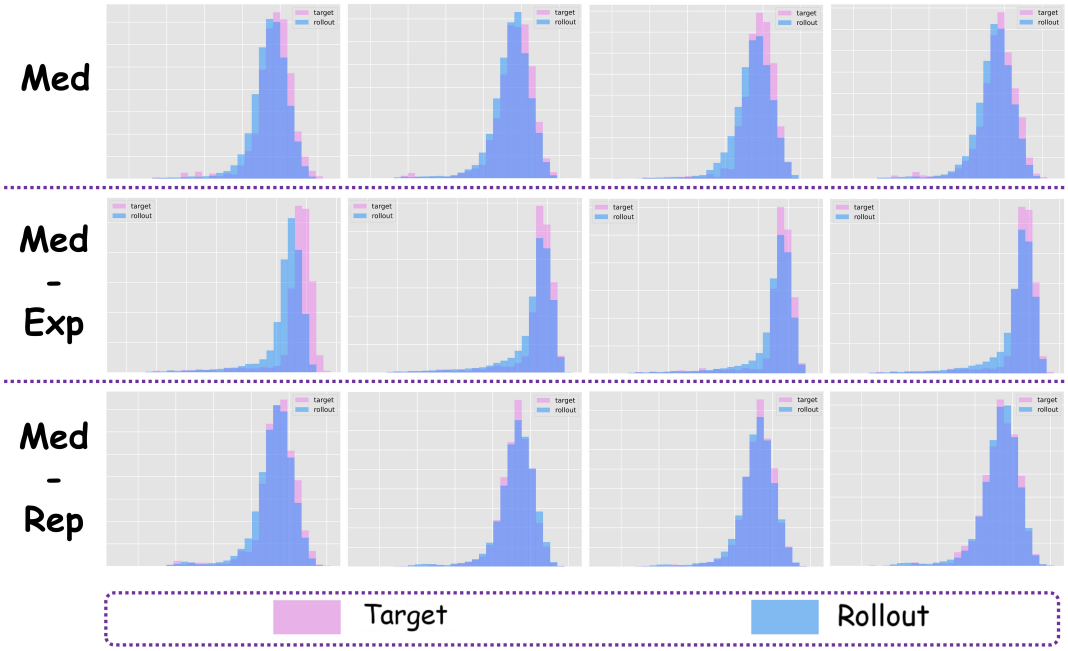

Figure 7: Within the **CEDC**, for the **HalfCheetah** task, additional visualizations of distribution histograms across three datasets.

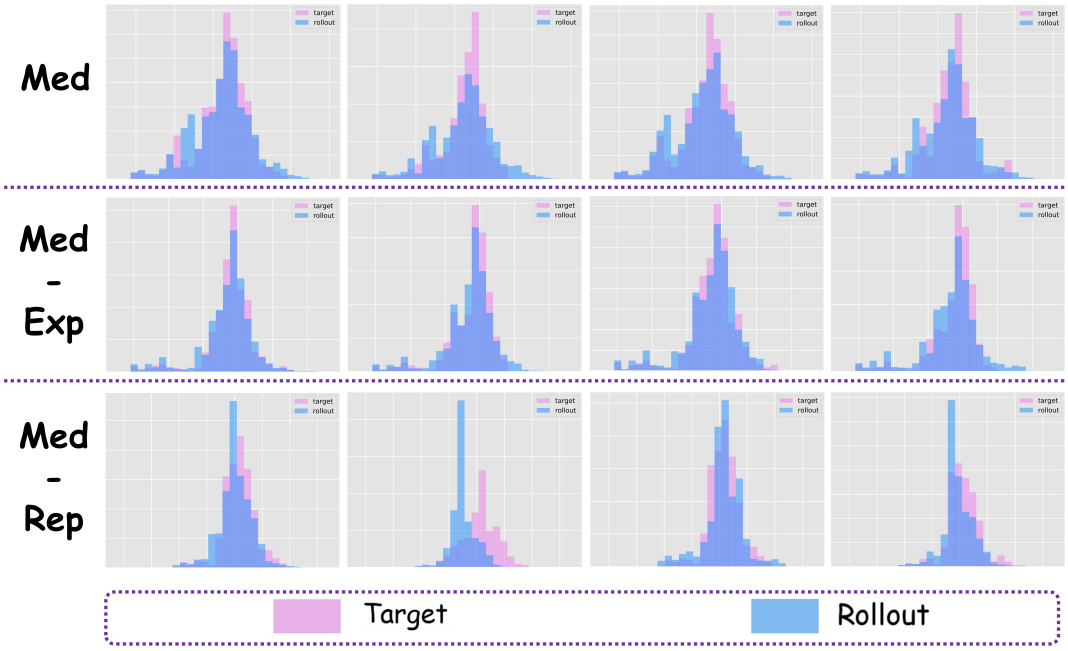

Figure 8: Within the **CEDC**, for the **Hopper** task, additional visualizations of distribution histograms across three datasets.

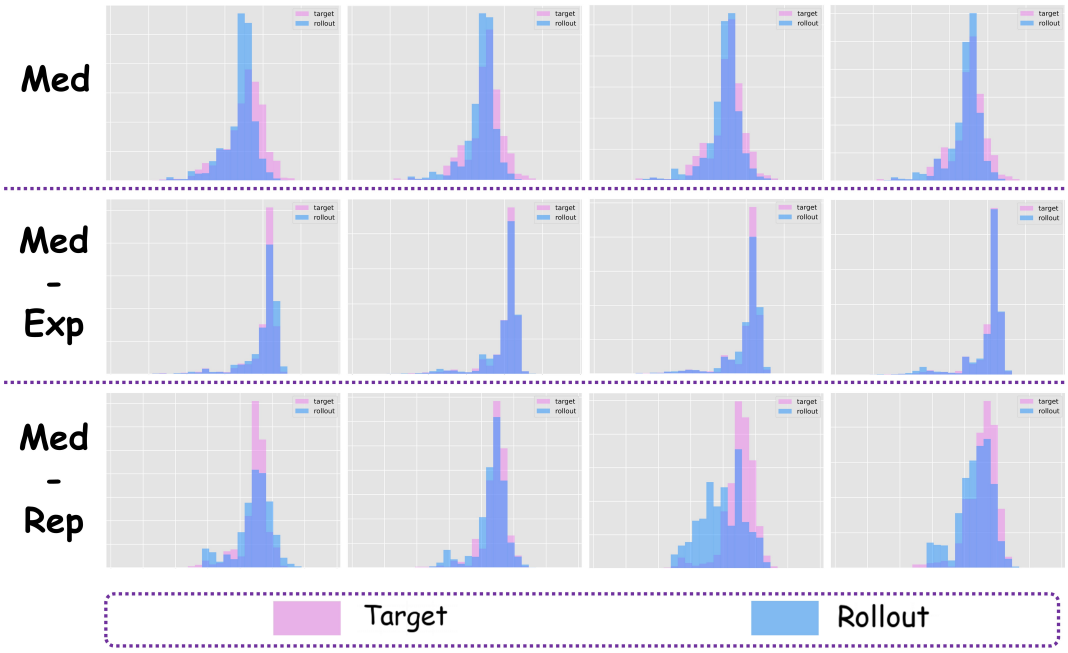

Figure 9: Within the **CEDC**, for the **Walker2d** task, additional visualizations of distribution histograms across three datasets.

Calibrated Enhanced Decision Mamba (CEDMamba): Figure 10 (HalfCheetah), Figure 11 (Hopper), Figure 12 (Walker2d).

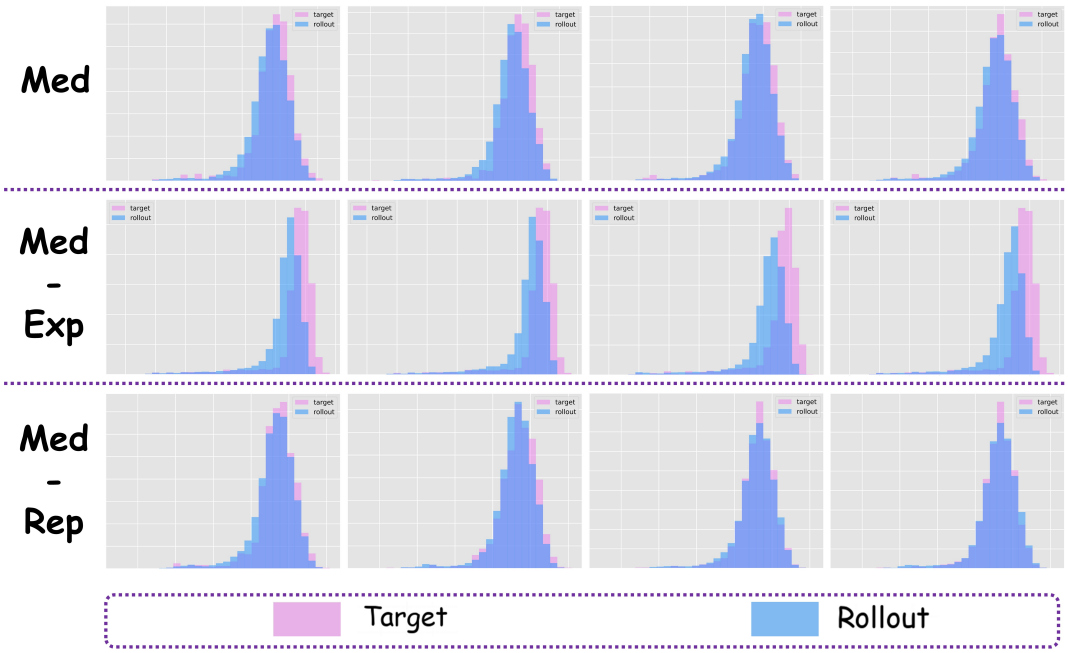

Figure 10: Within the **CEDMamba**, for the **HalfCheetah** task, additional visualizations of distribution histograms across three datasets.

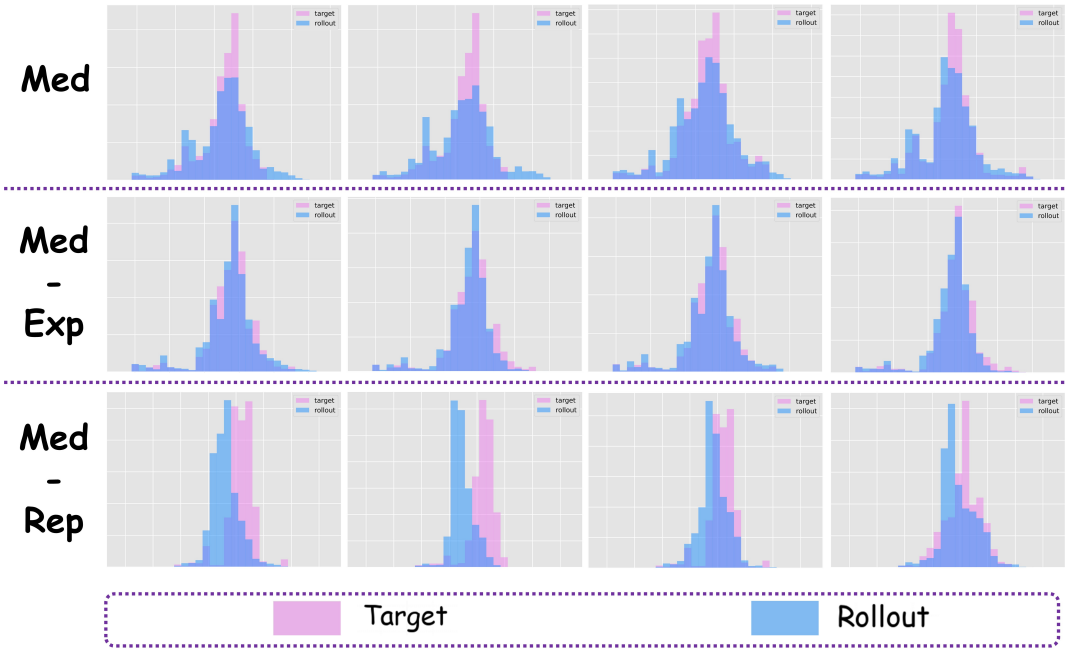

Figure 11: Within the **CEDMamba**, for the **Hopper** task, additional visualizations of distribution histograms across three datasets.

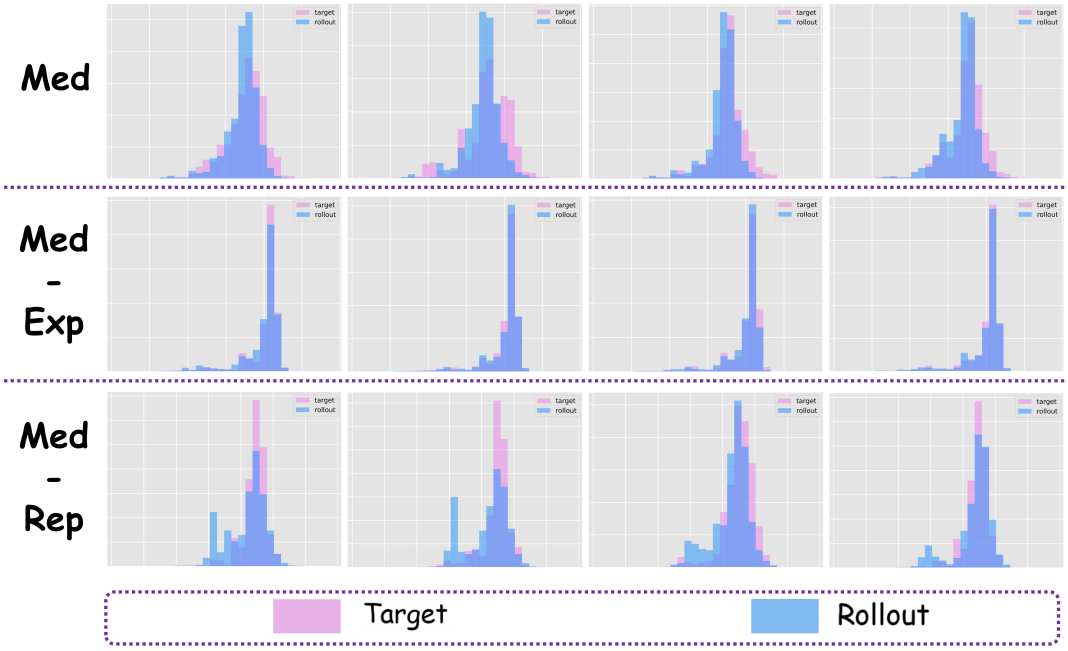

Figure 12: Within the **CEDMamba**, for the **Walker2d** task, additional visualizations of distribution histograms across three datasets.

C Details of Case Studies

C.1 Dataset and Benchmark.

The MuJoCo environment (Todorov et al., 2012) is part of the D4RL benchmark (Fu et al., 2020), encompassing a series of continuous locomotion tasks characterized by dense reward signals. In our case studies, we focus on three specific tasks: HalfCheetah (**HC**), Hopper (**Hp**), and Walker2d (**Wk**). To facilitate a unified representation of returns across tasks, normalization is performed to the return:

$$\text{Return} = 100 \times \frac{\text{Score} - \text{Random Score}}{\text{Expert Score} - \text{Random Score}}.$$

For each of these, we utilize three different v2 datasets, each representing a different level of data quality: medium (**Med**), medium-expert (**Med-Exp**), and medium-replay (**Med-Rep**). The medium dataset contains one million samples generated by a policy operating at roughly one-third of an expert's performance level. The medium-replay dataset is derived from the replay buffer of a policy trained to emulate the medium policy's performance. And the medium-expert dataset combines one million samples from the medium policy with an additional million from an expert policy. Overall, MuJoCo offers an excellent testing ground to investigate how datasets, originating from policies with varying skill levels, influence learning and performance.

C.2 Baselines.

Decision Transformer (DT) frames offline reinforcement learning as a sequence modeling problem, and leveraging the Transformer architecture. Instead of optimizing the value functions or the learning policies directly, DT treats the trajectories as sequences composed of states, actions, and returns-to-go (the sum of future rewards from each step). The model (agent) is trained to predict the next action, conditioning on the previous states, actions, and desired return of the trajectory. At each timestep, input into the Transformer consists of a tuple: the current state, the previous action, and the target return-to-go (RTG). It then autoregressively predicts the next action that should be taken to maximize the likelihood of achieving the return. Such an approach effectively turns policy generation into a sequence generation task, similar to how language models predict the next word in a sentence.

Decision ConvFormer (DC) serves as a novel offline reinforcement learning (RL) predictor that fundamentally rethinks how sequential dependencies are captured in offline reinforcement learning trajectories. While the traditional DT models offline reinforcement learning as a sequence modeling problem using the Transformer's self-attention mechanism, DT's reliance on attention can be suboptimal for offline RL tasks. Furthermore, the Decision ConvFormer (DC) replaces the global attention mechanism with local, causal 1D convolutional filters. Specifically, DC employs three independent convolutional mixers for states, actions, and returns, each operating over a local temporal window (e.g., 6 timesteps). This design ensures that predictions are made using only nearby tokens, effectively capturing the local, Markovian structure of RL data, while also dramatically reducing model complexity and computational cost.

Decision Mamba (DMamba) further replaces the self-attention mechanism in DT with the Mamba (Gu & Dao, 2024) block. The architecture comprises token-mixing and channel-mixing layers, with the Mamba block acting as the primary token-mixing module. By leveraging the structured state space modeling, Decision Mamba potentially offering greater efficiency and the ability to model longer dependencies.

C.3 Implementation Details.

To ensure the reproducibility of the experiment, we have included all codes in the supplementary materials. Herein, we encounter important hyperparameters and implementation details. All experiments are conducted on a single NVIDIA GeForce RTX 3090 graphics card. Hyperparameters are mainly set with reference to the Categorical Decision Transformer (Furuta et al., 2022). In Table 4, we list detailed hyperparameters of the Calibrated Enhanced Decision Transformer (CEDT). In Table 5, we list detailed hyperparameters of the Calibrated Enhanced Decision ConvFormer (CEDC). In Table 6, we list detailed hyperparameters of the Calibrated Enhanced Decision Mamba (CEDMamba).

Table 4: Hyperparameters for the Calibrated Enhanced Decision Transformer (CEDT).

Hyperparameters	Value
Number of Bins	31
Number of Layers	3
Number of Attention Head	1
Embedding Dimension	128
Batch Size	64
Context Length	20
Dropout	0.1
Learning Rate	1e-4
Grad Norm Clip	0.25
Weight Decay	1e-4
Warmup Steps	10000
Activation Function	ReLU
Gamma	1.0
Max Training Iterations	10
Random Seeds	0, 1, 2, 3, 4

Table 5: Hyperparameters for the Calibrated Enhanced Decision ConvFormer (CEDC).

Hyperparameters	Value
Number of Bins	31
Number of Layers	3
Convolution Window Size	6
Embedding Dimension	128
Batch Size	64
Context Length	20
Dropout	0.1
Learning Rate	1e-4
Grad Norm Clip	0.25
Weight Decay	1e-4
Warmup Steps	10000
Activation Function	ReLU
Gamma	1.0
Max Training Iterations	10
Random Seeds	0, 1, 2, 3, 4

Table 6: Hyperparameters for the Calibrated Enhanced Decision Mamba (CEDMamba).

Hyperparameters	Value
Number of Bins	31
Number of Layers	3
Embedding Dimension	128
Batch Size	64
Context Length	20
Dropout	0.1
Learning Rate	1e-4
Grad Norm Clip	0.25
Weight Decay	1e-4
Warmup Steps	10000
Activation Function	ReLU
Gamma	1.0
Max Training Iterations	10
Random Seeds	0, 1, 2, 3, 4